Journal of Materials Chemistry B

ROYAL SOCIETY OF CHEMISTRY

PAPER

View Article Online
View Journal | View Issue

Cite this: J. Mater. Chem. B, 2024, 12, 9050

Mid-infrared passive spectroscopic imaging for visualizing tooth quality

So Yamashita,[a] Masahiro Okada, *[bc] Takuya Matsumoto [b] and Ichiro Ishimaru*[a]

Although the measurement of tooth quality is necessary for precise prediction of caries formation, typical measurement methods include tooth-hardness measurements and absorption spectroscopy, which generally use infrared light irradiation. These methods are destructive or invasive, and obtaining two-dimensional information in the oral cavity is difficult. Mid-infrared emissions from the surface of an object reflect intrinsic vibrations of molecules in the object. In this study, a mid-infrared passive spectroscopic imaging system was developed using an inexpensive uncooled microbolometer array sensor with an optimized multi-slit, which eliminated the cancellation of interference intensities between two adjacent emission points, to obtain two-dimensional information from an object without external infrared light irradiation. First, the feasibility of obtaining two-dimensional information on tooth quality using the proposed system was examined, and emission spectra attributed to phosphate ions in hydroxyapatite (HAp), the main component of enamel, were successfully obtained from bovine teeth. Further, the hardness of bovine teeth was measured, and a correlation (R^2 = 0.8067) between the Vickers hardness and peak area ratio of phosphate ions assigned to the crystalline and amorphous phases of a tooth was established. Additionally, tooth-hardness visualization in a non-contact manner was demonstrated as two-dimensional information using the obtained regression equation.

Received 9th February 2024,
Accepted 11th August 2024

DOI: 10.1039/d4tb00280f

rsc.li/materials-b

1. Introduction

With dental research advancements leading to a global decline in the prevalence of dental caries,[1,2] the focus of dental research will shift to developing preemptive therapy for caries formation after achieving precise prediction for sound and noncavitated tooth surfaces with new evaluation methods.

Tooth enamel is a highly mineralized tissue comprising a non-stoichiometric form of hydroxyapatite (HAp). Erosion of tooth enamel by acidic drinks and foods causes tooth softening due to demineralization,[3,4] which increases the risk of caries formation.[5–7] As enamel surface softening is an early manifestation of erosion,[8] the risks of caries formation on enamel surfaces can be quantified through hardness measurements. However, such measurements involve destructive tests and entire tooth surfaces cannot be measured owing to point analysis. Additionally, no information on the structural changes that occur at the molecular or atomic level of enamel surfaces during erosion is provided.[9]

Usually, alterations in the mechanical properties (including hardness) of erosive enamel are accompanied by chemical composition and/or structural changes in surfaces. Numerous techniques including microradiography, chemical analysis, microscopy methods, secondary ion mass spectroscopy, and quantitative light-induced fluorescence have been used to investigate chemical changes mostly *in vitro*.[10–12] Infrared absorption spectroscopy has been extensively studied as a non-destructive method using Fourier-transform infrared (FT-IR) spectroscopy;[13,14] however, this technique is invasive because the infrared light irradiation causes heat generation[15] and obtaining two-dimensional (2-D) information using FT-IR spectroscopy is difficult.

Recently, we developed a mid-infrared passive spectroscopic imaging system using an imaging-type 2-D Fourier spectrometer.[16,17] Our system employed an inexpensive uncooled microbolometer array sensor, and the optimized multi-slit grating to prevent bright spot cancellations was used to acquire 2-D spectral information from weak light emitted from a target without external light irradiation. The mid-infrared passive spectroscopic imaging system is expected to obtain compositional and/or molecular-level structural changes two-dimensionally and non-invasively, and our previous study is the first to detect light emission from glucose molecules present in the human body two-dimensionally using the system in a non-contact manner.[18] Furthermore, a strong

[a] Graduate School of Science for Creative Emergence, Kagawa University, 2217-20 Hayashi-cho, Takamatsu-City, Kagawa 761-0396, Japan. E-mail: ishimaru.ichiro@kagawa-u.ac.jp
[b] Department of Biomaterials, Faculty of Medicine, Dentistry and Pharmaceutical Sciences, Okayama University, 2-5-1 Shikata-cho, Kita-ku, Okayama City, Okayama 700-8558, Japan
[c] Division of Dental Biomaterials, Tohoku University Graduate School of Dentistry, 4-1 Seiryo-machi, Aoba-ku, Sendai 980-8565, Japan. E-mail: masahiro.okada.c2@tohoku.ac.jp

correlation between the intensity of light emitted from glucose and the blood glucose concentration measured by an invasive sensor from the wrist at regular intervals was established.[18] Hence, our system is anticipated to find applications in real-time monitoring of diabetic patients (to detect hypoglycemic attacks during sleep or hyperglycemia in a population). This innovative mid-infrared passive spectroscopic imaging system is also expected to enable the measurement of a wide variety of objects including inorganic materials and hard biological tissues.

This study is the first to visualize changes two-dimensionally in the tissue quality (*i.e.*, tooth hardness) accompanied by structural changes using the mid-infrared passive spectroscopic imaging system. Initially, we measured a bovine enamel and evaluated the possibility of obtaining information on tooth composition or structure. Thereafter, we investigated the correlation between the acquired emission spectrum and tooth hardness measured using a Vickers hardness tester. Finally, we visualized tooth hardness two-dimensionally from tooth emission spectrum using a regression equation between them.

2. Experimental

2.1. Instrumentation

The configuration diagram of the mid-infrared passive spectroscopic imaging system used in this study is illustrated in Fig. 1. The system comprised a 2-D light-receiving device, lens system (imaging, objective, and interchangeable lenses) for focusing the light emitted from a target onto the detection surface, and variable phase shifter installed in the optical system. Boson 320 microbolometer (Teledyne FLIR, Tokyo, Japan) used in thermographic cameras was employed as a detector. Ge aspherical lenses (focal length (F) = 15 mm, diameter (d) = 25 mm) were used as the imaging and objective lenses. Another Ge aspheric lens (F = 15 mm; d = 50 mm) was used as an interchangeable lens. The system employed a multi-slit to eliminate cancellation of interference intensities between two adjacent emission points.[19] As a result, the sensitivity of the system was higher than that of Michelson interferometers used in general FT-IR spectroscopy.[17] The variable phase shifter comprised fixed and moving mirrors (size = 15 × 30 mm^2 each) coated with gold to exhibit high reflectance over a wide wavelength range, from ultraviolet to infrared. A part of the light emitted from the local target area was reflected by the fixed mirror, while the rest was reflected by the movable mirror; these two lights interfered at the detector. The interference intensity was dependent on the mirror position. An interferogram was obtained from a continuous measurement of interference intensity at a specific pixel on the detector for which the target was in focus while operating the moving mirror. The spectrum at the specified pixel was obtained by Fourier transformation of the interferogram. A 2-D spectroscopic image was obtained by performing the aforementioned procedure for all pixels in the 2-D array detector. The measurement band of the device ranged from 1428 to 714 cm^{-1} in wavenumber (7 to 14 μm in wavelength), and the number of pixels of the detector was 320 × 256.

2.2. Mid-Infrared passive spectroscopic imaging for bovine tooth

The digital photographs of the optical system and bovine tooth (approximately 6 × 4 × 2 mm^3 with ∼1 mm thick enamel and ∼1 mm thick dentine) used for experiments are shown in Fig. 2. For this study, permanent bovine mandibular incisors, without any cracks or carious defects, collected from a slaughterhouse were used owing to their morphological similarity to human teeth.[20] The bovine teeth were trimmed/grinded with #1000 silicon carbide abrasive papers and the enamel side was polished with 1 μm alumina under pure water irrigation followed by ultrasonic washing thrice with pure water for 10 s and removing excess water with filter paper before use. As shown in Fig. 2A, the optical system comprised the spectroscope described in Section 2.1 and interchangeable Ge lens (d = 50 mm, F = 0.5) with an infinite conjugate ratio. The distance between the target and interchangeable lens was set to 200 mm, and the field of view was 35 × 20 mm^2. Each measurement required 40 s, and four measurements were performed for each sample (total measurement time = 160 s). Four interferograms on a pixel obtained from four 40-sec measurements were averaged, and a 2-D interferogram image was obtained after averaging 20 × 20 pixels in the image. In the first experiment, three areas with high interference intensities in the teeth were selected (Fig. 3A), and the spectra were obtained after Fourier transformation.

2.3. Investigation of the correlation between tooth hardness and emission spectra

To investigate the relationship between tooth hardness and the emission spectra obtained using mid-infrared passive spectroscopic

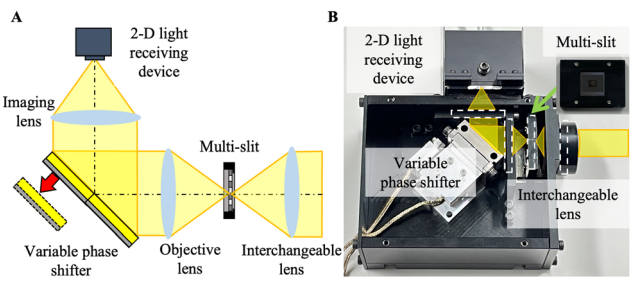

Fig. 1 Experimental setup. (A) An illustration of the basic structure and (B) a digital photograph of imaging- type 2-D Fourier spectrometer.

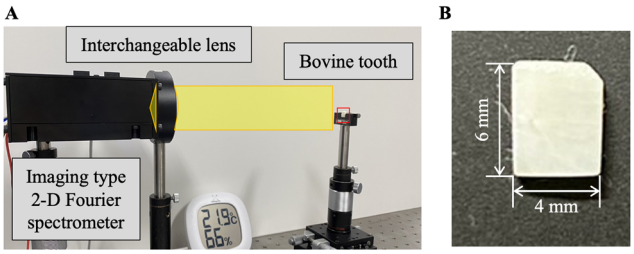

Fig. 2 Measurement of bovine tooth by mid-infrared passive spectroscopic imaging. Digital photographs of (A) the experimental setup and (B) a bovine tooth sample used in this study.

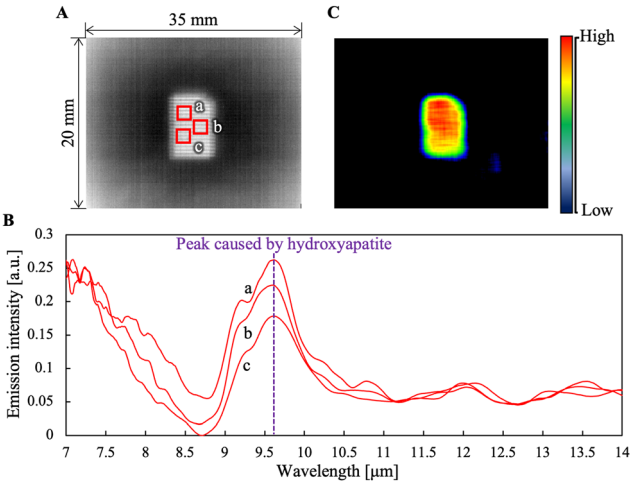

Fig. 3 Mid-infrared passive spectroscopic imaging of a bovine tooth enamel. (A) Mid-infrared image without variable phase shifter operation. (B) Emission spectra at points (a)–(c) indicated in Fig. 3A. (C) Pseudo-color image obtained by subtracting the background emission intensity at 8.7 μm from the phosphate-derived peak intensity at 9.6 μm.

imaging, the phosphate-derived emission peak at a wavelength of 9.6 μm in each spectrum was deconvoluted into crystalline and amorphous phases[21] using a software (MagicPlot, Ver. 3.0.1, MagicPlot Systems, LLC, Saint Petersburg, Russia). The area ratios of the peaks assigned to the crystalline and amorphous phases were calculated. Vickers hardness of each tooth was measured at 100 gf for 15 s using a microhardness tester (FM-700; Future-Tech Corp., Kanagawa, Japan). Mid-infrared passive spectroscopic imaging measurements and hardness tests were performed on the same teeth at their central position (1.5 × 1.5 mm), and 30 bovine teeth of different hardness (150–350 HV) were evaluated in this study. Furthermore, the effects of acid erosion on teeth hardness and spectra were evaluated, where 12 bovine teeth (258 ± 41 HV) were immersed in 1.0 mL of 0.03 mol L^{-1} citric acid (Nacalai Tesque Inc., Kyoto, Japan) for 5, 15, 30, or 60 min (N = 3 for each immersion time) and analyzed following the aforementioned procedure.

2.4. Visualization of bovine tooth hardness from emission spectra

Tooth hardness was visualized two-dimensionally from the emission spectra of the tooth obtained using mid-infrared passive spectroscopic imaging. Visualization was conducted before and after a drop (6 μL) of 0.03 mol L^{-1} citric acid solution was set at the center (~2 mm in diameter) of the teeth (6 × 4 mm^2) at room temperature, followed by washing with pure water and removing the excess water with filter paper. The 2-D hardness was observed as a color map based on the hardness estimated from a regression equation obtained from the procedure described in Section 2.3. In this experiment, the 2-D interferogram image was obtained after averaging 6 × 6 pixels in the image.

3. Results

3.1. Mid-infrared passive spectroscopic imaging measurements for bovine teeth

The mid-infrared image obtained without variable phase shifter operation is shown in Fig. 3A. The tooth emitted light, while obvious contrast could not be observed within the tooth. The emission spectra at the points (a–c) shown in Fig. 3A are presented in Fig. 3B. Attributed to phosphate ions in HAp,[22] an emission peak at 9.6 μm was detected in each spectrum. By subtracting the emission intensity at 9.6 μm from the background intensity at 8.7 μm, the presence of the tooth was clearly confirmed, as shown in Fig. 3C. Thus, mid-infrared passive spectroscopic imaging was confirmed to detect bovine teeth and information on the chemical composition or molecular structure could be obtained from the emission spectrum.

3.2. Relationship between teeth hardness and emission spectrum

As shown in Fig. 4A, the phosphate-derived peaks between 900 and 1200 cm^{-1} (between 11.1 and 8.4 μm in wavelength, respectively) could be deconvoluted into six components:[21] symmetric (ν_1) P–O stretching component at ~950 cm^{-1} (10.5 μm in wavelength) of phosphate ions in amorphous

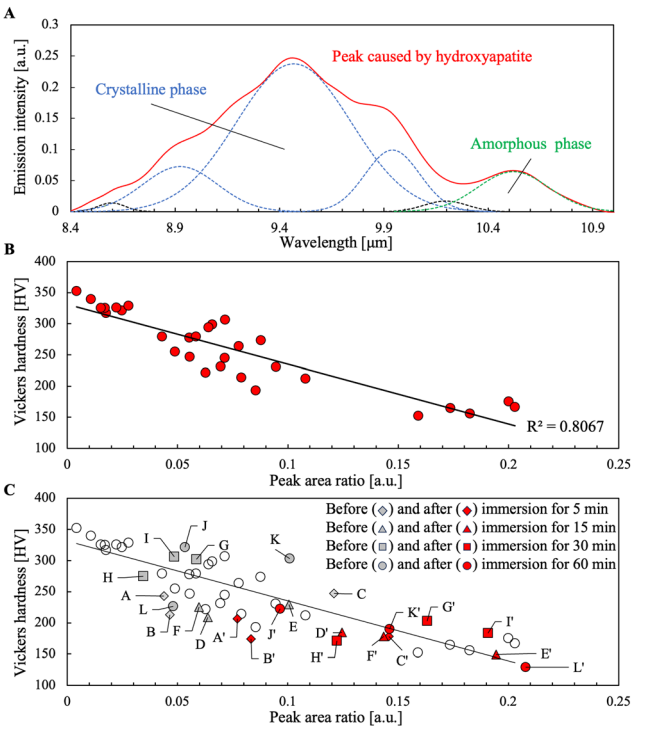

Fig. 4 Relationship between tooth hardness and emission spectrum assigned to crystalline and amorphous calcium phosphate. (A) Emission peak after deconvolution into six peaks based on a previous study.[21] (B) Correlation between peak area ratio of amorphous to crystalline and Vickers hardness of teeth. (C) Correlation between tooth hardness and peak area ratio of amorphous to crystalline before and after immersion of tooth in citric acid solution. The same alphabets (*e.g.*, A and A′) indicate the same sample before and after immersion.

calcium phosphate; three anti-symmetric (ν_3) P–O stretching components at ~1010, 1050, and 1110 cm^{-1} (9.9, 9.5, and 9.0 μm in wavelength, respectively) of phosphate ions in crystalline HAp; and two components at ~1150 and 980 cm^{-1} (8.7 and 10.2 μm in wavelength, respectively), which may both arise from HPO_4^{2-}.[21] In this study, the area ratio of the ν_1 component of amorphous calcium phosphate and the three ν_3 components of crystalline HAp showed a negative correlation (R^2 = 0.8067) with Vickers hardness. Furthermore, the samples after immersion in citric acid solution to reduce their hardness showed almost the same correlation, as shown in Fig. 4C. In Fig. 4C, the hardness after immersion for 5 min (A′–C′) was smaller than that for 60 min (J′), and the three hardness data points for 60 min (J′–L′) were scattered, which may reflect the difference in the initial hardness before immersion. Notably, no strong correlation was observed for the intensity at 9.6 μm before the deconvolution or the components of HPO_4^{2-} after the deconvolution (data omitted).

3.3. Two-dimensional visualization of bovine tooth hardness from emission spectra

In emission spectra (Fig. 5A) of the bovine teeth before and after dropping the citric acid solution at the center of teeth followed by washing with pure water and removing the excess water on the surface (Fig. 5B), the phosphate-derived peaks between 11.1 and 8.4 μm (in wavelength) changed after the drop. Using the regression line shown in Fig. 4B, hardness was estimated two-dimensionally as shown in Fig. 5C. From the obtained results, the change in hardness due to acid treatment was confirmed to be clearly detected by 2-D imaging.

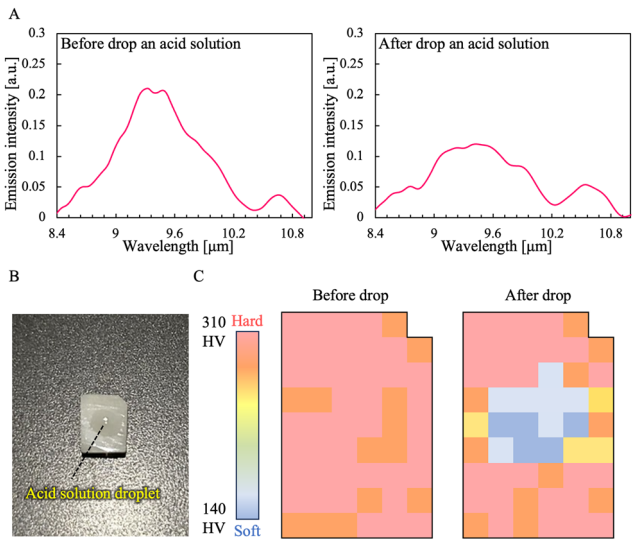

Fig. 5 Two-dimensional visualization of bovine tooth-hardness from the emission spectra. (A) Emission spectra of bovine tooth before and after dropping citric acid solution followed by washing with pure water and removing the excess water on the surface. (B) Digital photograph of citric acid solution droplet on a tooth before washing. (C) Visualization of bovine tooth hardness as a pseudo-color map from emission spectra at 53 locations on the bovine tooth.

4. Discussion

Generally, infrared spectroscopic imaging uses absorption spectroscopy that irradiates a target with external light and detects the light transmitted or reflected by the target.[23] In absorption spectroscopy, component information can be obtained from the absorbance spectrum calculated from the energy loss of external light by the intrinsic vibrations of molecules in the target.[23] Therefore, some limitations to absorption spectroscopy exist: the measurement is invasive as light source is a heat source[15] and measurement of three-dimensional objects is difficult due to the unevenness in light irradiation and detection angle.[24] Based on Planck's law, a mid-infrared light (~10 μm in wavelength) is emitted from the surface of a living body with an intensity corresponding to the body temperature (~300 K).[25] In mid-infrared passive spectroscopic imaging, component information can be obtained from emission spectrum, which reflects the intrinsic vibrations of molecules. Therefore, non-invasive measurements regardless of the surface topography are possible using mid-infrared passive spectroscopic imaging.

Thermal emission spectroscopy (TES)[26] is an antecedent mid-infrared passive spectroscopic imaging technique; however, TES is an expensive point-measurement method. The optical system of TES comprises a Michelson interferometer that uses mercury cadmium telluride (MCT) as the photodetector.[26] Therefore, the TES system is vulnerable to mechanical vibrations and is not portable. On the other hand, the imaging-type 2-D Fourier spectrometer used in this study is compact, inexpensive, and robust against mechanical vibration.[27] The 2-D spectral characteristics that eliminates the cancellation of interference intensity between bright spots can be obtained through the use of multi-slit grating. In this study, the measurement distance is fixed at 200 mm; however, theoretically, the measured performance of the spectrometer is considered independent of distance because the light emitted from the target is omni-directional. Hence, the areal density of light incident on the spectrometer from a single emission point decreases as the measurement distance increases (the areal density is inversely proportional to the square of the distance), whereas the field-of-view area per pixel increases in proportion to the square of the distance. These two relationships cancel the effect of distance, resulting in a distance-independent measurement.

In this study, mid-infrared passive spectroscopic imaging is performed on bovine teeth after polishing to remove organic contaminants from their surface. As emission intensities from objects are proportional to their volumes according to Planck radiation law, and the range of infrared absorption by organics is different from that of phosphate-derived absorption,[23] thin-layered organic contamination would not have a significant effect on the emission spectra.

In future, the motion of the target or spectroscope should be considered for further improvement because each measurement in this study requires 160 s and the measurements are performed for a fixed target. Since the spectroscope used in this

study has no tracking function to follow the movements or vibrations of the target during measurement, we are considering improvements in the image processing technology,[28–30] along with the introduction of a tracking system for moving objects.[31–33] Additionally, a direct measurement of teeth backside using the considered spectroscope is difficult owing to its size compared with the oral cavity. Therefore, we plan to use our one-shot Fourier spectrometer,[34] whose size is the same as a bean, inside the oral cavity.

Since the characteristic emission at ~9.6 μm (in wavelength) of the bovine tooth is attributed to enamel crystals, the deconvolution of the characteristic emission into crystalline HAp and amorphous calcium phosphate phases correlates tooth hardness with the peak area of the amorphous phase relative to that of the crystalline phase (the ratio of amorphous to crystalline). According to a previous study,[21] the crystallinity or crystal size of HAp is related to the hardness of teeth and bones; our procedure for tooth hardness visualization from emission spectra is based on the same phenomenon. Furthermore, the deconvolution of each spectrum in this study is performed manually; however, correlations between emission spectrum and hardness can be achieved using machine learning[35] after collecting a large amount of data.

This study demonstrated the 2-D qualification of sound and non-cavitated tooth surfaces by our system, and our system is also expected to be useful for the quality evaluation of artificially mineralized (armored) tooth surfaces by several methods such as laser-assisted biomineralization methods[36,37] in the patient's oral cavity.

There are three major limitations in this study. First, teeth trimmed to approximately 1 mm thick enamel with 1 mm dentin at the bottom were used in this study. Hence, future study should check the effects of enamel thickness and the dentin condition. Second, the mid-infrared spectral imaging was performed in air at room temperature. Therefore, future study should check the effects of humidity and temperature. Third, bovine teeth were used in this study. Hence, future study should reconfirm the findings by conducting larger-scale studies with human teeth in oral cavities with generalizing the findings and applying them to real situations.

5. Conclusions

We investigate the use of mid-infrared passive spectroscopic imaging for 2-D visualization of tooth hardness. The emission peaks are attributed to the phosphate ions in crystalline HAp, the main component of teeth, and amorphous calcium phosphate. Additionally, we observe a negative correlation between tooth hardness and the peak area ratio of the amorphous phase to the crystalline phase. The results of this study can be used to predict the risk of caries formation non-invasively and conveniently.

Author contributions

S. Yamashita: formal analysis, investigation, data curation, visualization and writing – original draft; M. Okada: conceptualization, methodology, formal analysis, investigation, data curation, writing – original draft, funding acquisition and project administration; T. Matsumoto: conceptualization, validation, writing – review & editing, supervision and funding acquisition; I. Ishimaru: methodology, software, validation, writing – review & editing and supervision.

Data availability

All relevant data are within the manuscript. The data are available from the corresponding author on reasonable request.

Conflicts of interest

There are no conflicts to declare.

Acknowledgements

This work was financially supported by KAKENHI (grant numbers: JP24K02626, JP22H03274 and JP23H00235) from the Japan Society for the Promotion of Science and by CREST (grant Number: JPMJCR22L5) from the Japan Science and Technology Agency. We would like to thank Editage (**https://www.editage.jp**) for English language editing.

Notes and references

1 C. H. Splieth, R. M. Santamaria, R. Basner, E. Schüler and J. Schmoeckel, *Caries Res.*, 2019, **53**, 609–616.
2 R. M. Santamaria, J. Schmoeckel, R. Basner, E. Schüler and C. H. Splieth, *Caries Res.*, 2019, **53**, 659–666.
3 A. Lussi, N. Schlueter, E. Rakhmatullina and C. Ganss, *Caries Res.*, 2011, **45**, 2–12.
4 M. Low and A. Alhuthali, *Mater. Sci. Eng., C*, 2008, **28**, 1322–1325.
5 D. L. Gambon, H. S. Brand and E. C. I. Veerman, *Br. Dent. J.*, 2012, **213**, 55–57.
6 D. Tantbirojn, A. Huang, M. D. Ericson and S. Poolthong, *J. Dent.*, 2008, **36**, 74–79.
7 H. Eimar, E. Ghadimi, B. Marelli, H. Vali, S. N. Nazhat, W. M. Amin, J. Torres, O. Ciobanu, R. F. Albuquerque Junior and F. Tamimi, *Acta Biomater.*, 2012, **8**, 3400–3410.
8 M. C. D. N. J. Huysmans, H. P. Chew and R. P. Ellwood, *Caries Res.*, 2011, **45**, 60–68.
9 X. Wang, A. Klocke, B. Mihailova, L. Tosheva and U. Bismayer, *J. Phys. Chem. B*, 2008, **112**, 8840–8848.
10 M. E. Barbour and J. S. Rees, *J. Dent.*, 2004, **32**, 591–602.
11 S. Houari, K. DeRocher, T. T. Thuy, T. Coradin, V. Srot, P. A. van Aken, H. Lecoq, T. Sauvage, E. Balan, J. Aufort, M. Calemme, N. Roubier, J. Bosco, K. Jedeon, A. Berdal, D. Joester and S. Babajko, *Acta Biomater.*, 2023, **169**, 155–167.
12 T. Walsh, R. Macey, D. Ricketts, A. Carrasco Labra, H. Worthington, A. J. Sutton, S. Freeman, A. M. Glenny,

P. Riley, J. Clarkson and E. Cerullo, *J. Dent. Res.*, 2022, **101**, 261–269.
13 F. C. Besic, S. O. Zimmerman and M. R. Wiemann, *J. Dent. Res.*, 1962, **41**, 718.
14 J. Reyes-Gasga, E. L. Martínez-Piñeiro, G. Rodríguez-Álvarez, G. E. Tiznado-Orozco, R. García-García and E. F. Brès, *Mater. Sci. Eng., C*, 2013, **33**, 4568–4574.
15 M. Almeida, K. E. Torrance and A. K. Datta, *Int. J. Food Prop.*, 2006, **9**, 651–664.
16 Y. Inoue, I. Ishimaru, T. Yasokawa, K. Ishizaki, M. Yoshida, M. Kondo, S. Kuriyama, T. Masaki, S. Nakai, K. Takegawa and N. Tanaka, *Appl. Phys. Lett.*, 2006, **89**, 121103.
17 K. Nogo, K. Ikejima, W. Qi, N. Kawashima, T. Kitazaki, S. Adachi, K. Wada, A. Nishiyama and I. Ishimaru, *Anal. Methods*, 2021, **13**, 647–659.
18 T. Kitazaki, Y. Morimoto, S. Yamashita, D. Anabuki, S. Tahara, A. Nishiyama, K. Wada and I. Ishimaru, *Sci. Rep.*, 2022, **12**, 1–9.
19 Y. Suzuki, M. Fujiwara, P. Abeygunawardhana, W. Qi, N. Kawashima, I. Ishimaru, S. Suzuki, K. Wada, A. Nishiyama and S. Sato, *Appl. Opt.*, 2015, **54**, 6254–6259.
20 X. Hu, Y. Peng, C. P. Sum and J. Ling, *J. Endod.*, 2010, **36**, 2008–2011.
21 N. Pleshko, A. Boskey and R. Mendelsohn, *Biophys. J.*, 1991, **60**, 786–793.
22 L. Bachmann, R. Diebolder, R. Hibst and D. M. Zezell, *Appl. Spectrosc. Rev.*, 2003, **38**, 1–14.
23 A. Barth, *Biochim. Biophys. Acta - Bioenerg.*, 2007, **1767**, 1073–1101.
24 D. Cozzolino, *Comput. Electron. Agric.*, 2023, **212**, 108078.
25 B. B. Lahiri, S. Bagavathiappan, T. Jayakumar and J. Philip, *Infrared Phys. Technol.*, 2012, **55**, 221–235.
26 I. Notingher, P. Xiao, R. E. Imhof, E. P. Berg and F. C. Pascut, *Anal. Sci.*, 2002, **17S**, s486–s489.
27 H. Kobayashi, T. Kawajiri, K. Yanogawa, A. Nishiyama, N. Tanaka, S. Takahashi and I. Ishimaru, *Jpn. J. Opt.*, 2012, **41**, 36–44.
28 X.-C. Zhao, J.-Z. Yuan, H.-Z. Liu and J.-S. Zhou, *J. Softw.*, 2017, **12**, 53–61.
29 W. S. L. Jebarani and T. Kamalaharidharini, *Proceedings of 2017 International Conference on Intelligent Computing and Control (I2C2)*, Coimbatore, India, 2017, pp. 1–8, DOI: **10.1109/I2C2.2017.8321868**.
30 P. Forczmański and A. Smoliński, in *Computational Science – ICCS 2021, Lecture Notes in Computer Science*, ed. M. Paszynski, D. Kranzlmüller, V. V. Krzhizhanovskaya, J. J. Dongarra and P. M. Sloot, Springer, Cham, 2021, pp. 149–163, DOI: **10.1007/978-3-030-77977-1_12**.
31 M. A. Rashidan, S. N. Sidek and N. Rusli, *Proceedings of 12th International Congress on Advanced Applied Informatics (IIAI-AAI)*, Kanazawa, Japan, 2022, pp. 278–282, DOI: **10.1109/IIAIAAI55812.2022.00063**.
32 H. Ito, K. Oiwa and A. Nozawa, *Proceedings of 2018 International Conference on Intelligent Informatics and Biomedical Sciences (ICIIBMS)*, Bangkok, Thailand, 2018, pp. 6–7, DOI: **10.1109/ICIIBMS.2018.8549966**.
33 A. Kwásniewska, J. Rumiński and P. Rad, *Proceedings of 10th International Conference on Human System Interactions (HSI)*, Ulsan, Korea (South), 2017, pp. 41–47, DOI: **10.1109/HSI.2017.8004993**.
34 N. Kawashima, T. Kitazaki, K. Nogo, A. Nishiyama, K. Wada and I. Ishimaru, *Opt. Rev.*, 2020, **27**, 530–541.
35 T. Shan, F. R. Tay and L. Gu, *J. Dent. Res.*, 2021, **100**, 232–244.
36 A. Oyane, N. Saito, I. Sakamaki, K. Koga, M. Nakamura, A. J. Nathanael, N. Yoshizawa, K. Shitomi, K. Mayumi and H. Miyaji, *Mater. Sci. Eng., C*, 2019, **105**, 110061.
37 A. Oyane, I. Sakamaki, K. Koga, M. Nakamura, K. Shitomi and H. Miyaji, *Mater. Sci. Eng., C*, 2020, **116**, 111170.